

RESEARCH

Open Access



Pathological and molecular insights into intravenous leiomyomatosis: an integrative multi-omics study

Sheng Yin^{1†}, Peipei Shi^{1†}, Jing Han^{2†}, Hua Li^{3†}, Aimin Ren¹, Li Ma¹, Wenbin Tang¹, Wenxue Liu¹, Sihui Yu¹, Tingting Li¹, Chunsheng Wang^{3*}, Yingyong Hou^{2*} and Jiarong Zhang^{1*} 

Abstract

Intravenous leiomyomatosis (IVL) is a histologically well differentiated smooth muscle tumor with aggressive behavior, capable of extending throughout the venous system. Understanding how IVL occurs and develops is really important for diagnosing and treating it. Unfortunately, because IVL is quite rare, there aren't many comprehensive studies available. In our research, we carried out an extensive multi-omics study, gathering tissue samples from IVL cases, uterine fibroid, and normal myometrium. The single-cell RNA sequencing analysis revealed a notable difference in cell composition between IVL and uterine fibroid. Additionally, H&E staining demonstrated more frequent hydropic changes and hyalinization in IVL tissues, along with a reduced vascular density compared to both normal myometrium and uterine fibroid. In our proteomics analysis of eight paired samples of IVL and normal myometrium fresh frozen tissue, we identified proteins that were differentially expressed, mainly related to focal adhesions and regulation of the actin cytoskeleton. The most frequently involved chromosomes included deletions in 10q22.2, 10q24.32, 13q14, and 13q21-31. Correlation analyses highlighted chromosome 10q as the most frequent cytoband, with corresponding proteins involved in regulating focal adhesions and the cytoskeleton. Integrated analysis between pathological and clinical characteristics indicated that chromosome 10q deletion and vascular morphology in IVL could serve as important markers predicting aggressive behavior. Our study sheds light on the pathological and molecular changes linked to IVL, which could pave the way for new treatment approaches.

Keywords Intravenous leiomyomatosis, Multi-omics analysis, Chromosome 10q deletion, Vascular morphology, Aggressive behavior

[†]Sheng Yin, Peipei Shi, Jing Han and Hua Li contributed equally to this work.

*Correspondence:
Chunsheng Wang
wang.chunsheng@zs-hospital.sh.cn
Yingyong Hou
hou.yingyong@zs-hospital.sh.cn

Jiarong Zhang
zhang.jiarong@zs-hospital.sh.cn
¹Department of Obstetrics and Gynecology, Zhongshan Hospital, Fudan University, Shanghai, China
²Department of Pathology, Zhongshan Hospital, Fudan University, Shanghai, China
³Department of Cardiac Surgery, Zhongshan Hospital, Fudan University, Shanghai, China



Introduction

Intravenous leiomyomatosis (IVL) is an uncommon smooth muscle tumor characterized by histologically well-differentiated smooth muscle disease but exhibiting aggressive behavior [1]. Typically originating in the uterus, IVL extends along the venous system to the iliac vein, inferior vena cava (IVC), right heart, and occasionally the pulmonary artery, resulting in diverse clinical symptoms and, at times, sudden death. Traumatic surgery is imperative for the removal of extra-pelvic disease [2].

Two theories exist regarding the origin of IVL: one predominant theory suggests that IVL originates from uterine fibroid (UF), while the other posits that IVL stems from the smooth muscle cells (SMCs) of the vessel walls [3–5]. Although new research methods and animal models for understanding how diseases happen keep coming up all the time [6, 7], limited research has been conducted on IVL tumorigenesis. Ordulu et al. classified IVL into cellular, vascular and usual type based on microscopic characteristics. Their array comparative genomic hybridization studies revealed frequent genetic alterations involving chromosomes 1p, 22q, 2q, 13q, and 14q [8]. Lu et al. utilized Sanger sequencing and short tandem repeat analysis, observed discordance in Mediator complex subunit 12 (MED12) mutation, microsatellite instability, and loss of heterozygosity between UF and IVL [9]. Other studies employing MED12 gene sequencing confirmed IVL as a distinct tumor from UF [10, 11]. At the transcriptional level, Zhang et al. identified differentially expressed genes between IVL and UF, primarily enriched in the extracellular matrix, cell adhesion, and steroid hormone stimulus [12]. Despite these findings, comprehensive multi-omics studies investigating IVL tumorigenesis and development are lacking.

In this investigation, we initiated single-cell RNA sequencing (scRNA-seq) to delineate the cell types in a paired set of UF and IVL fresh tissues. Subsequently, hematoxylin and eosin (H&E) as well as immunohistochemistry (IHC) staining were conducted on 23 paired IVL and normal myometrium paraffin-embedded samples. This aimed to delve deeper into the pathological changes characteristic of IVL, with results validated through an additional cohort. To unveil the molecular alterations in IVL, we employed integrated omics analyses, encompassing tandem mass tag (TMT)-based quantitative proteomics analysis and Whole-Exome Sequencing (WES). This comprehensive approach was applied to eight paired IVL samples (featuring extra-pelvic disease) and normal myometrium fresh frozen tissue. Finally, an integrated analysis was performed, bridging the gap between pathological observations and clinical characteristics. This study not only shed light on the pathological and molecular features associated with IVL tumorigenesis and tumor behavior but also charted new avenues for the treatment of this disease.

Methods

Ethics

Our study adhered to the principles of the Declaration of Helsinki and received approval from the ethical committee of Zhongshan Hospital, Fudan University (Ethics Committee document number: B2021-488R). Written informed consent was obtained from all participating patients.

Study flowchart and tissue sample Collection

The study's flowchart is illustrated in Fig. 1. Patients pathologically diagnosed with IVL at Zhongshan Hospital, Fudan University, between 2014 and 2020 were included. For scRNA-seq, samples were acquired from

Diagram: multi-omics study in IVL

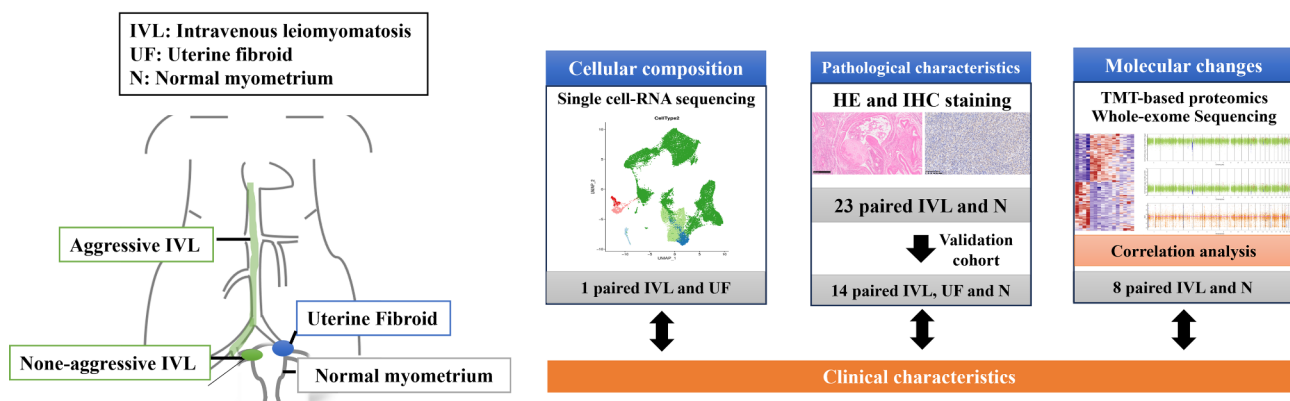


Fig. 1 Overview of the experimental design

freshly removed tissues, including one paired UF and IVL. TMT-based proteomic and WES analyses were performed on eight paired fresh frozen samples, comprising IVL lesions (both extracted from the IVC) and corresponding normal myometrium. These samples were collected during multidisciplinary surgical procedures and stored at -80°C until use. For H&E and IHC staining, 23 IVL and paired normal myometrium tissues were collected and embedded in paraffin. The validation cohort included 14 paired normal myometrium, uterine fibroid, and IVL tissues. All samples underwent reconfirmation by qualified pathologists, and comprehensive medical records were meticulously reviewed and collected.

Single-cell RNA sequencing

In brief, cells were loaded onto the 10X Chromium Single Cell Platform (10X Genomics) at a concentration of 1,000 cells per μL , using the Single Cell 3' library and Gel Bead Kit v.3, following the manufacturer's protocol. The process involved the generation of gel beads in emulsion (GEMs), barcoding, GEM-RT clean-up, complementary DNA amplification, and library construction, all in accordance with the manufacturer's instructions. Library quantification was performed using Qubit before pooling, and the final library pool was sequenced on an Illumina Novaseq 6000 instrument. The targeted mean reads per cell was set to $\geq 25,000$, and our samples achieved an average of 31,222 reads per cell.

Data processing of single-cell RNA-seq from chromium system

The cellranger software (version 2.1.0) was utilized for mapping to the GRCh38 human genome, performing quality control, and counting reads of Ensembl genes using default parameters.

Unsupervised clustering and visualization

Unsupervised clustering was conducted using R with the Seurat package (version 2.2). Genes expressed in fewer than two cells were excluded. Cells with more than 200 genes and less than 10% mitochondrial genes were subjected to further processing. Subsequently, the coefficient of variation of genes was calculated using Seurat. Dimensionality reduction of the data was conducted through principal component analysis, focusing on the first 2000 genes with the highest variability. A k-nearest neighbor graph was constructed based on Euclidean distances within the space defined by the first 10 principal components. The Louvain Modularity optimization algorithm was employed to cluster the cells within the graph, and the resulting clusters were visualized using t-distributed Stochastic Neighbor Embedding (tSNE) projection. Cells expressing high levels of genes encoding hemoglobin were removed from the analysis.

Marker gene identification and cell-type annotation

The 'bimod' test implemented in the Seurat FindMarkers function was utilized to compute the differential expression of each cluster. Genes exhibiting a \log_2 average expression difference of 0.585 and a significance level of $P < 0.05$ were designated as marker genes. Canonical markers of established cell types were employed to annotate cell clusters. Seurat-Bimod statistical test was used to find differentially expressed genes between each group of cells and other groups of cells ($\text{FDR} \leq 0.05$ and $|\log_2 \text{Fold Change}| \geq 1.5$). The TopGO R package was utilized for Gene Ontology (GO) enrichment analysis of these significantly differentially expressed genes, while the Hypergeometric test in R was employed for Kyoto Encyclopedia of Genes and Genomes (KEGG) pathway enrichment analysis. GO terms and KEGG pathways that were significantly enriched were identified based on a threshold FDR (adjusted P-value) ≤ 0.05 .

TMT protein labeling and bioinformatics analysis

Following the extraction of total protein from the samples, a portion of the protein was utilized for determining concentration and SDS-PAGE analysis, while another portion underwent trypsin hydrolysis and labeling. Equal amounts of each labeled protein sample were amalgamated for chromatographic separation, facilitating liquid chromatography tandem mass spectrometry (LC-MS/MS) analysis. The qualitative and quantitative data obtained were subjected to analysis. Expression level analysis and functional analysis were conducted subsequent to quality evaluation and preprocessing. The functional annotation encompassed the use of several common data analysis tools, including GO and KEGG pathway analysis. Interaction analysis was then executed for the differentially expressed proteins (DEPs) identified. Furthermore, correlation analysis, expression pattern clustering, and Venn analysis were performed, and heat maps were generated to enhance data interpretation and visualization.

Whole exosome sequencing

Qualified DNA samples underwent random fragmentation into 150 to 220 bp fragments using Covaris. Subsequently, the Agilent SureSelect Human All Exon V6 kit was employed for library construction and capture. The library assembly involved various steps, including DNA end-joining, addition of polyA tails, incorporation of sequencing adapters, purification, magnetic bead capture, PCR amplification, and other processes. A thorough re-evaluation of raw data quality was conducted, considering parameters such as error rate, data volume, comparison rate, and coverage. The resulting high-quality sequences were aligned to the GRCh37.p13 human

genome to detect sample variation information, which was subsequently analyzed.

Integrated multi-omics analysis of IVL

To harmonize data across multiple platforms, we compiled a list of all genes exhibiting copy number variation (CNV) and their associated proteins. Correlation (Pearson P-value) was calculated, with significance set at $P < 0.05$. Enrichment analyses, including GO and KEGG pathway analyses, were performed for positively correlated CNVs/proteins. In exploring the potential molecular mechanisms of IVL tumorigenesis, we enriched the frequency of chromosome positions and analyzed the corresponding proteins within the altered CNVs/proteins.

H&E and IHC staining

Archival paraffin blocks from 23 IVL patients, along with paired normal myometrium samples, were meticulously chosen for this study. Sections of 4 μm thickness were obtained from the paraffin-embedded samples, and subsequent H&E and IHC staining procedures were conducted on these slides. For H&E staining, microscopic characteristics were thoroughly examined in each slide, encompassing the proportion of hydropic change and hyalinization, as well as vascular densities in the tumor parenchyma. Furthermore, all IVL cases were classified

based on cellular, vascular, and usual morphology. The extent of these morphological features was scored as minimal ($< 5\%$), focal (5–24%), or diffuse ($> 25\%$) following a prior study⁶. In the case of IHC staining, the final protein expression score was derived by multiplying the percentage of positive cells (PPC) with the intensity of staining (IS). PPC categories included: 0 = $< 10\%$ of positive cells, 1 = 10–25%, 2 = 25–50%, 3 = 50–75%, and 4 = $\geq 75\%$ of positive cells. IS was classified as 0 (negative), 1 (weakly positive), 2 (moderately positive), and 3 (strongly positive). The cumulative score was then categorized as “low” for scores ranging from 0 to 3, “medium” for scores between 4 and 7, and “high” for scores from 8 to 12. Random fields under the 100x microscope were selectively chosen for vessel calculation.

The specific protocol for this study is summarized in the Supplemental Methods.

Results

IVL and UF exhibit profound differences in cellular composition through scRNA-seq

To delve into the cellular heterogeneity between IVL and UF, scRNA-seq profiles were generated from a paired IVL and UF tissue sample. The results, illustrated in Fig. 2A, unveiled the existence of 22 distinct clusters among high-quality cells. These 22 clusters were further categorized into eight subpopulations, encompassing fibroblasts,

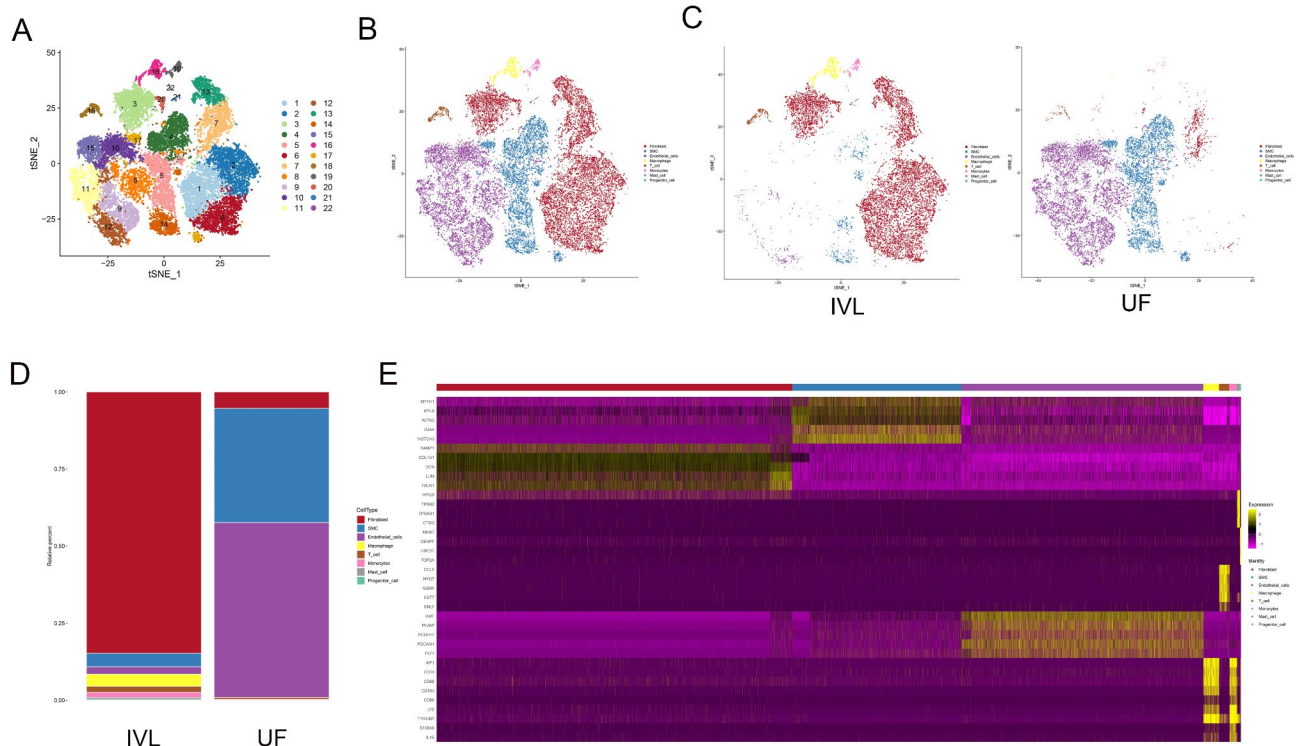


Fig. 2 Single-cell atlas of IVL and UF. **(A)** tSNE plot illustrating clusters of high-quality cells from IVL and UF. **(B)** Identification of cell lineages based on gene expression. **(C)** Annotation of cell clusters per sample. **(D)** Distribution of cells per sample. **(E)** Heatmap of gene expression analyzed by single-cell RNA sequencing, presenting key markers for each cell type. SMC, Smooth Muscle Cell

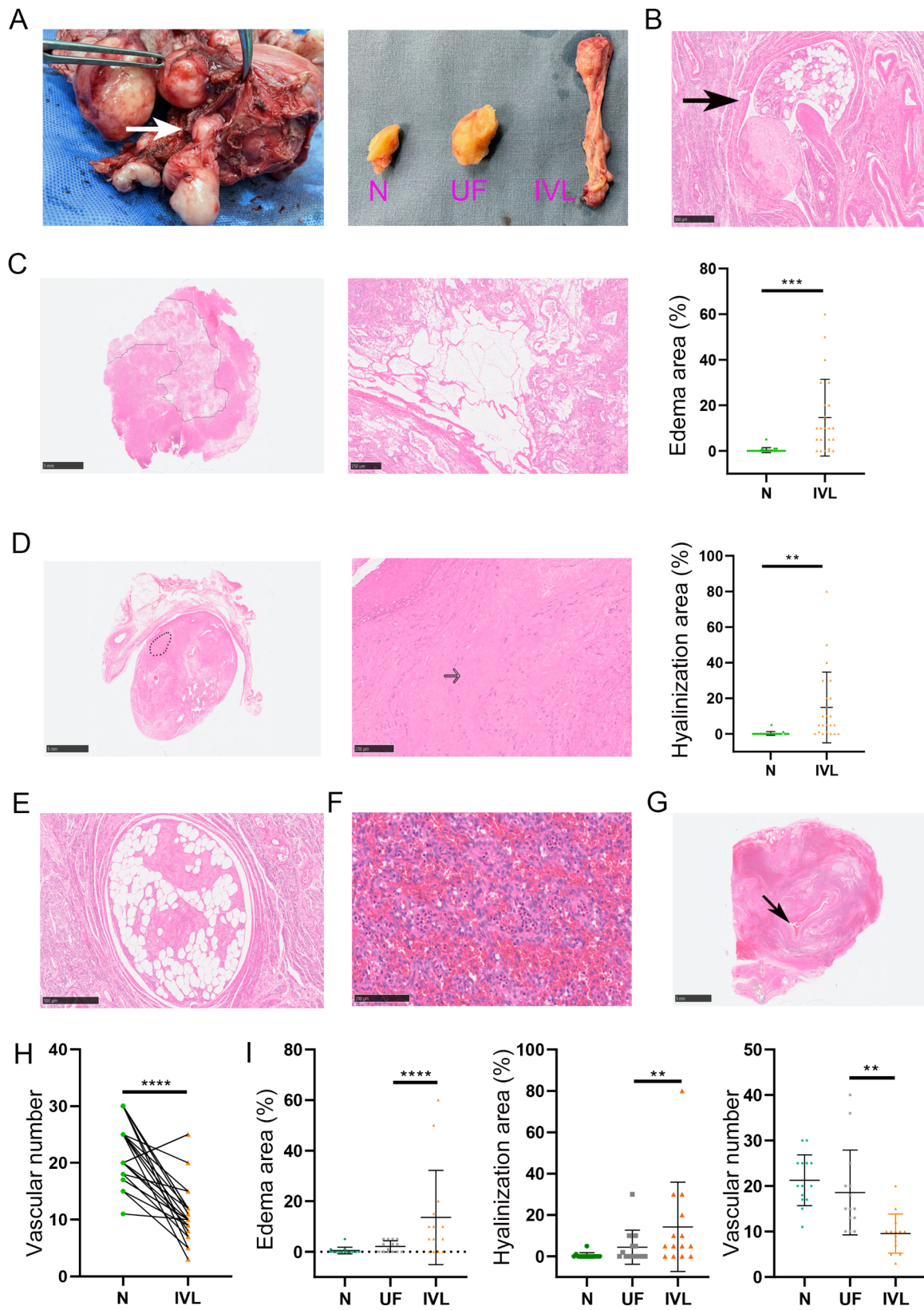


Fig. 3 (See legend on next page.)

(See figure on previous page.)

Fig. 3 Pathological characteristics in IVL. **(A)** Gross appearance of IVL. **(B)** Typical microscopic image of IVL. An intravascular tumour plug. **(C)** Edema change in IVL. The proportions of the edema area between normal myometrium and IVL. **(D)** Hyaline degeneration in IVL. The proportions of the hyaline degeneration between normal myometrium and IVL. **(E)** The adipose tissue in IVL. **(F)** Focal hemorrhage and neutrophils in IVL. **(G)** Thick vascular wall in IVL. **(H)** Vascular number between normal myometrium and IVL. **(I)** The proportions of the edema area, hyaline degeneration and vascular number between N, UF and IVL

SMCs, endothelial cells, macrophages, T cells, monocytes, mast cells, and progenitor cells (Fig. 2B). Examining the distribution in Fig. 2C and D, fibroblasts dominated the cellular landscape of the IVL lesion, constituting 84.73% of the identified cells. SMCs and endothelial cells accounted for 4.38% and 2.37%, respectively. In contrast, the UF lesion exhibited a distinct composition, with endothelial cells comprising 56.64% and SMCs making up 37.02%, while fibroblasts constituted only 5.35%. These findings underscore a substantial cellular component disparity between IVL and UF, characterized by reduced levels of SMCs and a markedly increased prevalence of fibroblasts in IVL. Moreover, the observation of limited endothelial cells in IVL suggests a potential hypovascular characteristic. The heat map in Fig. 2E summarizes the top five expressed genes in each cluster. In conclusion, the single-cell analysis underscores the profound differences in cellular components between IVL and UF, emphasizing the necessity for a comprehensive exploration of the pathological and molecular changes associated with IVL.

Pathomorphological alterations in IVL

Subsequently, we scrutinized the pathomorphological distinctions between IVL and normal myometrium in a cohort of 23 IVL patients. The clinical attributes of these patients are succinctly outlined in Supplementary Table 1. Macroscopically, IVL exhibited a “worm-like” tissue appearance, softer in texture compared to both normal myometrium and UF (Fig. 3A). Histologically, IVL was characterized as a benign smooth muscle tumor located within venous vascular spaces (Fig. 3B). Pathomorphologically, numerous IVL tissues displayed hydropic changes and areas of hyalinization in proximity to the tumor parenchyma (Fig. 3C/D). In rare instances, adipose tissue was observed in IVL, accompanied by focal hemorrhage and neutrophil infiltration (Fig. 3E/F). Vascular morphology exhibited variability, with some instances featuring large vessels characterized by thick vascular walls (Fig. 3G).

Among the 23 IVL cases in our study, the prevailing morphology was vascular (16/23, 69.6%), followed by the cellular (2/23, 8.7%) and usual (2/23, 8.7%) types. Two patients exhibited a combination of cellular and vascular types, while one patient presented with both vascular and usual types.

Utilizing these morphological characteristics, we initially compared the hydropic change, hyalinization, and

vascular density in tumor parenchyma between IVL and normal myometrium. In IVL, 8 (34.8%), 10 (43.5%), and 5 (21.7%) patients exhibited hydropic changes as minimal, focal, and diffused, respectively, whereas only 4 patients (3 minimal and 1 focal) showed hydropic changes in normal myometrium. Hyalinization manifested as minimal, focal, and diffused in 7 (30.4%), 11 (47.8%), and 5 (21.7%) patients in IVL, respectively, while only 2 patients (1 minimal and 1 focal) displayed hydropic changes in normal myometrium. The findings imply that the proportions of hydropic change and hyalinization were significantly higher in IVL (Fig. 3C/D). The median blood vessel counts in IVL and normal myometrium tissues were 10 (range 3 to 25) and 20 (range 11 to 30), respectively, suggesting that blood vessel density in IVL was lower than that in normal myometrium ($P < 0.001$) (Fig. 3H).

To further investigate whether these morphological characteristics differed between IVL and UF, 14 paired normal myometrium, UF, and IVL tissues were selected. The results also indicated that hydropic change and hyalinization were more frequently observed in IVL tissue than in both normal myometrium and uterine fibroids. Conversely, the vascular density was decreased in IVL tissues compared to both normal myometrium and uterine fibroids (Fig. 3I). In summary, when compared with normal myometrium and uterine fibroids, the proportions of hydropic change and hyalinization areas were significantly increased, and the vascular density was decreased in IVL tissues.

Proteomic alterations between IVL and paired normal myometrium

To delve deeper into the molecular changes within IVL, we conducted TMT-based proteomic analysis and WES on eight paired IVL and normal myometrium tissues. The clinical characteristics of these eight patients are summarized in Supplementary Table 2. A total of 263 DEPs were identified, with 133 proteins (50.6%) being upregulated and 130 downregulated (Fig. 4A). The volcano plot and heat map illustrate the distribution of these DEPs (Fig. 4B/C and Supplementary Table 3).

Functional annotation analysis using GO was performed to gain a better understanding of the biological functions of the DEPs. As depicted in Fig. 4D, the most downregulated GO terms included cell-matrix adhesion, focal adhesion, and actin cytoskeleton, while the most upregulated GO terms included complement activation and extracellular exosome. Furthermore, KEGG

enrichment analysis indicated that the DEPs are primarily involved in the regulation of actin cytoskeleton, extracellular matrix (ECM)-receptor interaction, and complement and coagulation cascades (Fig. 4E and Supplementary Table 4/5). The downregulated proteins in the protein-protein interaction (PPI) network included vinculin (VCL), ACTIN1, and ACTA2 (α -SMA), while the upregulated proteins included C3, C4B, APOA1, APOB, and FN1 (Fig. 4F). Vinculin, a cytoskeletal protein associated with cell-cell and cell-matrix junctions, plays a crucial role in cell morphology and locomotion. To further validate the results of the proteomic analysis, IHC staining of Vinculin was performed on the 23 paired IVL and normal myometrium paraffin-embedded tissues. As shown in Fig. 4G, the expression of Vinculin was significantly lower in IVL than in normal myometrium.

Genetic variants between IVL and paired normal myometrium

WES was conducted to investigate the genetic variants between IVL and the corresponding normal myometrium. As illustrated in Fig. 5A, a total of 381 mutations were identified, with nonsynonymous mutations constituting the most frequent type (61.4%), followed by synonymous mutations (24.4%). Excluding synonymous mutations, a total of 239 potential driver mutations were identified, with a median of 25 mutations in each sample. The prominently mutated genes included PKD1, CAPN15, ZNF90, SNAPC4, and MUC4 (Fig. 5B), with a mutation frequency of 25.0% (2/8). Details of each mutated gene mentioned above are summarized in Supplementary Table 6.

Subsequently, we analyzed CNVs between the two groups. The cytobands of somatic CNVs for each IVL sample are depicted in Fig. 5C. As indicated, the most frequent deletions in chromosomes were concentrated in 10q22.2, 10q24.32, 13q14, and 13q21-31, and observed in 3 of 8 IVLs (37.5%). The top CNV cytobands of gain were observed in 8q24, 11q13, 12q24, 19q13, and 20q13, each of the top CNV cytobands are also observed in 3 of 8 IVLs (Fig. 5D).

Correlation analysis of TMT-based proteomics and WES

To consolidate the findings from both proteomic and WES analyses, we conducted Pearson correlation analysis. The P-value was <0.05 for 87 CNVs-DEPs, among which 47 exhibited particularly positive correlations (correlation value of >0) (Fig. 6A). GO analyses were subsequently employed to unravel the potential functions of these 47 CNVs-DEPs. As depicted in Fig. 6B, ECM organization, cell-matrix adhesion, focal adhesion, and integrin binding were the primary enrichments. Subsequently, we delved into the cytoband distributions corresponding to these 47 altered CNVs-DEPs. Of 47

highly correlated CNV-DEPs, 10 (21.3%) were located on chromosome 10q, linking cytoband deletion with lower protein levels (Fig. 6C). Comparing quantity of the 10 candidate proteins in IVL and paired normal myometrium revealed significant difference in 3 out of 10 proteins. The expression levels of GLUD1, PDLIM1, and SLK were notably decreased in IVL (Fig. 6D and E). Significantly, both PDLIM1 and SLK play roles in the regulation of focal adhesion. Intriguingly, in the TMT-based proteomic analysis, we observed that the gene for vinculin, a cytoskeletal protein enriched in focal adhesions, is also located on chromosome 10q. These findings suggest that a chromosome 10q deletion in IVL may lead to the downregulation of several proteins involved in the regulation of the actin cytoskeleton and focal adhesion.

Integrated analysis of clinical and pathological characteristics

To explore potential correlations between clinical characteristics and pathological changes, we scrutinized data from 23 IVL patients, stratified by the extent of tumor disease (as illustrated in Table 1). Among the 15 aggressive IVL patients (with extra-pelvic disease), 26.7% exhibited diffuse hyalinization, with an equal percentage showing hydropic changes. These manifestations were observed in 12.5% of patients with intra-pelvic disease. In the subgroup of eight patients with intra-pelvic disease, Vinculin high expression was identified in 37.5% of cases, while the proportion of Vinculin high expression was 13.3% (2/15) in aggressive IVL cases. Despite the small sample size limiting our ability to draw definitive conclusions about the relationship between IVL tumor extent and vinculin IHC staining score, the results suggest that lower vinculin protein expression levels may be positively correlated with a more advanced tumor stage.

Among eight non-aggressive IVL patients, cellular, vascular, and usual morphology were observed in 25%, 50%, and 12.5% of patients, respectively. Two patients exhibited both cellular and vascular features. In the group of 15 aggressive IVL patients, a total of 80% were categorized as having vascular morphology, with one patient displaying both vascular and usual features. These findings imply that vascular morphology constitutes a substantial proportion in aggressive IVL cases.

Discussion

IVL exhibits a higher degree of fibrosis and hyalinization compared to normal myometrium and UF

In a recent study involving scRNA-seq analysis of five unpaired UF and normal myometrium samples, the cellular composition showed no significant differences between the two groups [13]. In our study, utilizing UF tissue as a control, we observed a striking difference in cellular composition between one paired IVL and UF

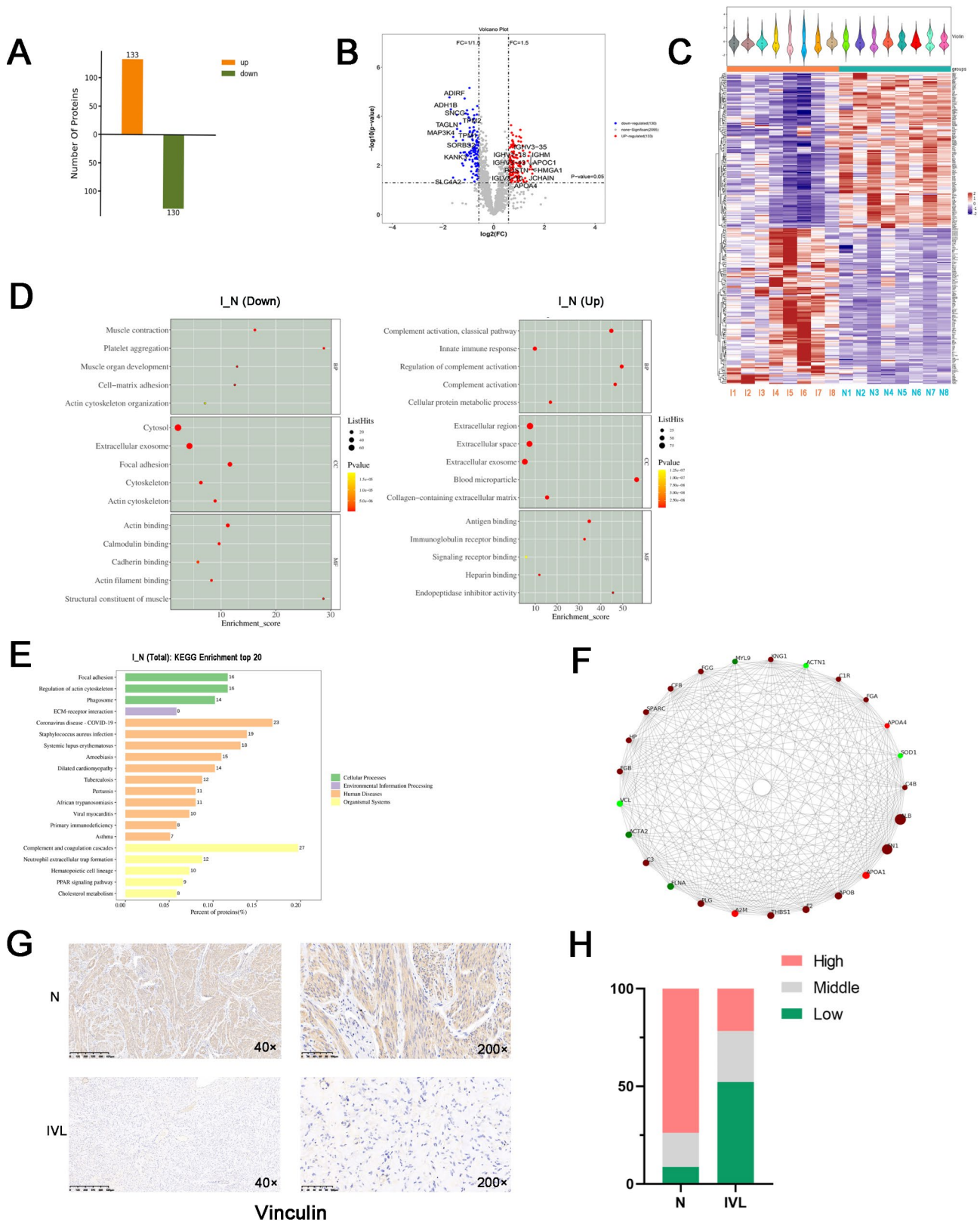


Fig. 4 (See legend on next page.)

(See figure on previous page.)

Fig. 4 Overview of the proteomics of IVL patients. **(A)** Visualization of 263 identified proteins, with orange indicating upregulated proteins and green indicating downregulated proteins. **(B)** Volcano Plot depicting significantly upregulated (red dots) and downregulated (blue dots) proteins, with gray dots representing proteins with no significant difference. The x-axis represents the fold change (Log2) between two groups, and the y-axis represents the p-value (-Log10) to illustrate the significance of differences. The top 10 upregulated and downregulated DEPs are labeled. **(C)** Heatmap for hierarchical clustering analysis of DEPs. Each row represents a protein, and each column indicates a sample. Colors indicate expression levels (red for high, purple for low). Violin plots depict the probability distribution of expression values. "+" denotes the median value, and the vertical axis represents protein expression. **(D)** GO Pathway Analyses of the top 15 enriched terms, classified by biological process (green), cellular component (blue), and molecular function (red). **(E)** Top 20 enriched KEGG terms, categorized into cellular processes (green), environmental information processing (purple), human disease (orange), and organismal systems (yellow). **(F)** PPI Network of the top 25 DEPs. DEPs are represented as dots, and edges between proteins indicate potential interactions. Dot size corresponds to combined interaction scores identified by Cytoscape. **(G)** Vinculin staining in IVL and normal myometrium. **(H)** Vinculin IHC staining score analysis

tissue through scRNA-seq. Specifically, there was a notable decrease in SMCs and an increase in fibroblasts in IVL. These findings were corroborated by our proteomic analysis, demonstrating a significant decrease in α -SMA (SMCs marker) and an increase in FN1 (fibroblasts marker) in IVL tissue. It's worth noting that although we initially dissected three paired UF and IVL fresh tissues for scRNA-seq, only one was successfully tested due to the low percentage of tumor cells in IVL tissue. The other two attempts failed because of inadequate cellular numbers, potentially linked to the increased fibrotic and hyalinized nature of IVL tissue.

HE staining revealed a significant increase in the proportions of hydropic change and hyalinization areas in IVL tissues compared to normal myometrium. While hydropic change and hyalinization are features also found in UF, we conducted a comparative analysis to discern differences between IVL and UF in terms of these histological features. The results further indicated a higher prevalence of hydropic change and hyalinization in IVL compared to both normal myometrium and UF. Given that hyalinization involves the transformation of a hard, cellular tumor into softer, acellular material, our findings provide insights into the clinical observation that IVL is noticeably softer than both normal myometrium and UF.

One of the primary functions of fibroblasts is the synthesis of collagen proteins [14, 15]. Collagen, a significant component of the extracellular matrix, contributes to the formation of a three-dimensional meshwork, providing physical support to cells and maintaining structural integrity in tissues [16]. Beyond its role in structural support, collagen plays a crucial role in various cellular processes, including cell migration, adhesion, angiogenesis, tissue development, and repair. Studies by Sahai E have highlighted that during migration, cancer cells utilize collagen fibers as tracks to leave the primary tumor, emphasizing the modulatory role of collagen in cell behavior [17]. Additionally, collagen has been identified as a novel driver of tumor invasion, promoting local invasion and metastasis [18, 19].

In our study, fibroblasts were predominantly identified in IVL. Upon comparing IVL with normal myometrium tissues and UF, we observed higher proportions

of hyalinization areas. These areas, characterized by the replacement of smooth muscle cells with collagen, exhibited a similar transformation in blood vessels within regions of hyaline necrosis [20]. Proteomic analysis further revealed an upregulation of proteins associated with collagen and ECM, most probably associated with the increased fraction of fibroblasts in IVL and the tumor's invasiveness.

In summary, our findings lead us to conclude that IVL exhibits more fibrotic and hyalinization features than normal myometrium and UF. These characteristics may be associated with the tumor development observed in IVL.

IVL exhibits a poorer blood supply compared to normal myometrium and UF

Our scRNA-seq results indicated significantly lower proportions of endothelial cells in IVL compared to UF. Additionally, HE staining results confirmed a lower blood vessel density in IVL compared to normal myometrium and UF. These findings suggest that IVL experiences inadequate blood supply, potentially explaining the higher frequency of hyalinization in IVL. Insufficient blood supply within the myoma is recognized as a key factor contributing to hyalinization. Interestingly, our results diverge from a previous study suggesting that IVL tumors possess a strong ability to promote angiogenesis. The earlier study proposed that IVL tumors exhibit upregulated expression of proangiogenic factors, including GATA1, LIF, CXCL8, SH2D2A, et al. [21].

To further investigate angiogenesis-associated pathway changes in IVL, we conducted a thorough analysis by identifying enriched angiogenesis-related terms in the GO analysis based on our proteomic data. DEPs associated with GO: 0016525 (negative regulation of angiogenesis) demonstrated significant upregulation in IVL. Notably, APOH (Apolipoprotein H; fold change=1.72), THBS1 (Thrombospondin 1; fold change=1.79), HRG (Histidine Rich Glycoprotein; fold change=1.60), THBS4 (Thrombospondin 4; fold change=2.19), and THBS2 (Thrombospondin 2; fold change=1.68) exhibited substantial increases in expression.

Conversely, DEPs associated with GO: 0045766 (positive regulation of angiogenesis) displayed significant downregulation in IVL. Noteworthy examples include HSPB1 (Heat Shock Protein Family B Member 1; fold change = 0.58), RRAS (RAS Related; fold change = 0.59), and AQP1 (Aquaporin 1; fold change = 0.61), all showing marked decreases in expression. Additionally, proteins involved in the general process of angiogenesis (GO: 0001525) underwent significant changes in IVL, with MYH9 (Myosin Heavy Chain 9; fold change = 0.66), FN1 (Fibronectin 1; fold change = 1.93), TGFBI (Transforming Growth Factor Beta Induced; fold change = 1.72), and APOD (Apolipoprotein D; fold change = 1.58) exhibiting altered expression levels.

Collectively, these results align with our earlier findings, supporting the notion that IVL experiences a poor blood supply in comparison to normal myometrium. However, to validate and further elucidate this conclusion, additional studies are warranted.

Dysregulation of focal adhesion and the actin cytoskeleton appears to be closely associated with the development of IVL

Our TMT-based proteomic analysis revealed that the most significantly downregulated signaling pathway was related to the regulation of the actin cytoskeleton and focal adhesion. Notably, key actin cytoskeletal proteins such as vinculin, α -actinin 1, Filamin A, and others exhibited downregulation. Focal adhesions, crucial for ECM interactions, play a fundamental role in maintaining tissue homeostasis and have been implicated in cancer development and pathogenesis [22, 23]. The disassembly of focal adhesions in cells has been linked to cytoskeletal transmission, promotion of epithelial-mesenchymal transition, and induction of cell migration [24–26], all of which contribute to cancer formation and progression.

A prior study conducted RNA-seq to explore differentially expressed genes between IVL and normal uterine muscle tissues. Consistent with our proteomic findings, the results from this study also suggested that IVL may disrupt the homeostasis of gene networks involved in ECM and cytoskeleton regulation [12]. These collective observations underscore the potential significance of focal adhesion and actin cytoskeletal dysregulation in the pathogenesis of IVL, emphasizing the need for further investigation into these molecular mechanisms.

Chromosome 10q deletions and vascular morphology could be important markers predicting the aggressive behavior of IVL

WES outcomes revealed an enrichment of chromosome deletions at specific loci, including 10q22.2, 10q24.32, 13q14, and 13q21-31, within IVL tissues. Correlation analyses unveiled that the deletion of chromosome 10q in

IVL might lead to the downregulation of proteins crucial in the regulation of the actin cytoskeleton and focal adhesion, which could play a significant role in IVL tumorigenesis. The validity of these findings was substantiated through vinculin IHC staining. Additionally, our investigation unveiled a correlation between lower vinculin protein expression and the distinct vascular morphology with the aggressive behavior observed in IVL.

Chromosome 10q deletions have been implicated in various diseases, including cutaneous T-cell lymphoma [27], low-grade gliomas [28], and prostate cancer [29]. A prior study by Ordulu et al. further supported the association of a 10q deletion in IVL lesions [8, 30]. In Ordulu's research, hierarchical clustering analysis identified three groups, with all IVL instances in group 3 ($n=5$) exhibiting a deletion on 10q. Notably, 80% of IVL cases in group 3 displayed aggressive behavior. In our study, the removal of all eight IVL tissues for TMT-based proteomic and WES from the inferior vena cava already signaled their aggressive nature. Furthermore, Ordulu's study highlighted that 80% of cases with a vascular morphology among the 5 IVL instances associated with recurrence, aligning with our results where 80% (12 out of 15) of aggressive IVL patients exhibited vascular morphology. Collectively, these findings strongly suggest that chromosome 10q deletions and vascular morphology serve as crucial markers for predicting the aggressive behavior of IVL.

Conclusion

Our study sought to investigate the pathological and molecular alterations in IVL patients through a comprehensive multi-omics approach. However, the study is subject to several limitations that warrant attention in future research. Firstly, the impact of our findings is constrained by the availability of only one paired IVL and UF sample for scRNA-seq. Secondly, to prevent the overinterpretation of IVL origin, further validation of WES results, including genetic variations, is essential with a larger sample size. Lastly, additional basic research is imperative to enhance our understanding of the origin and development of IVL.

In summary, this pioneering study conducted an integrated analysis, incorporating scRNA-seq, H&E, and IHC staining, TMT-based quantitative proteomics analysis, and WES of IVL. Our investigation unveiled both the pathomorphological and molecular characteristics in IVL, paving the way for new avenues in basic research and clinical treatment for IVL.

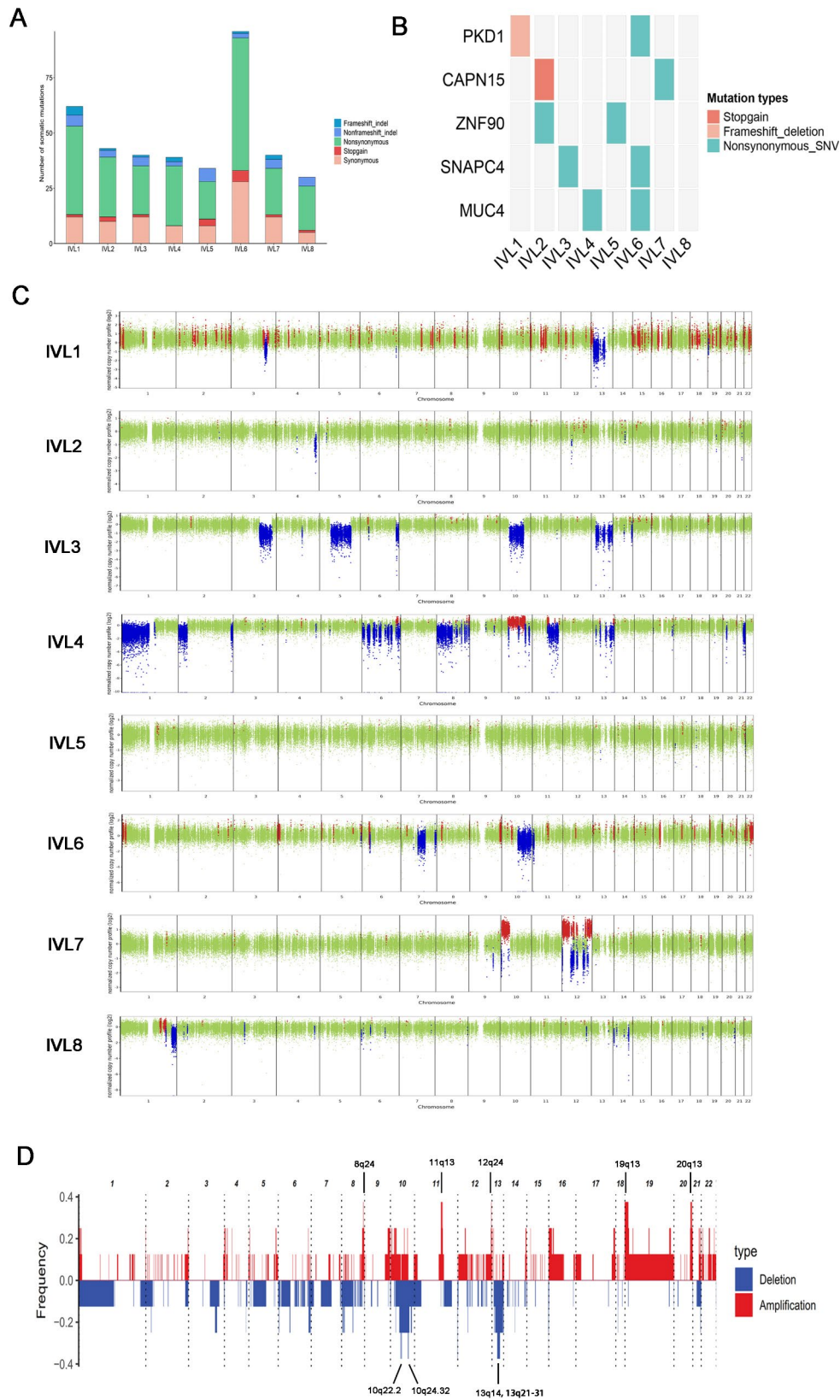


Fig. 5 Genomic profiles based on WES. **(A)** Representation of different mutational events in all IVL lesions. **(B)** Identification of the top 5 mutated genes corresponding to 8 samples. **(C)** Characteristics of genome-wide Copy Number Variations (CNVs) distribution in 8 samples, with a pooled analysis at the bottom. Red, blue, and green indicate amplification, deletion, and no change, respectively. X-axis represents chromosome cytoband, and Y-axis represents copy ratio (log2). **(D)** Overall chromosomal distribution of CNVs, where blue represents deletion and red represents amplification

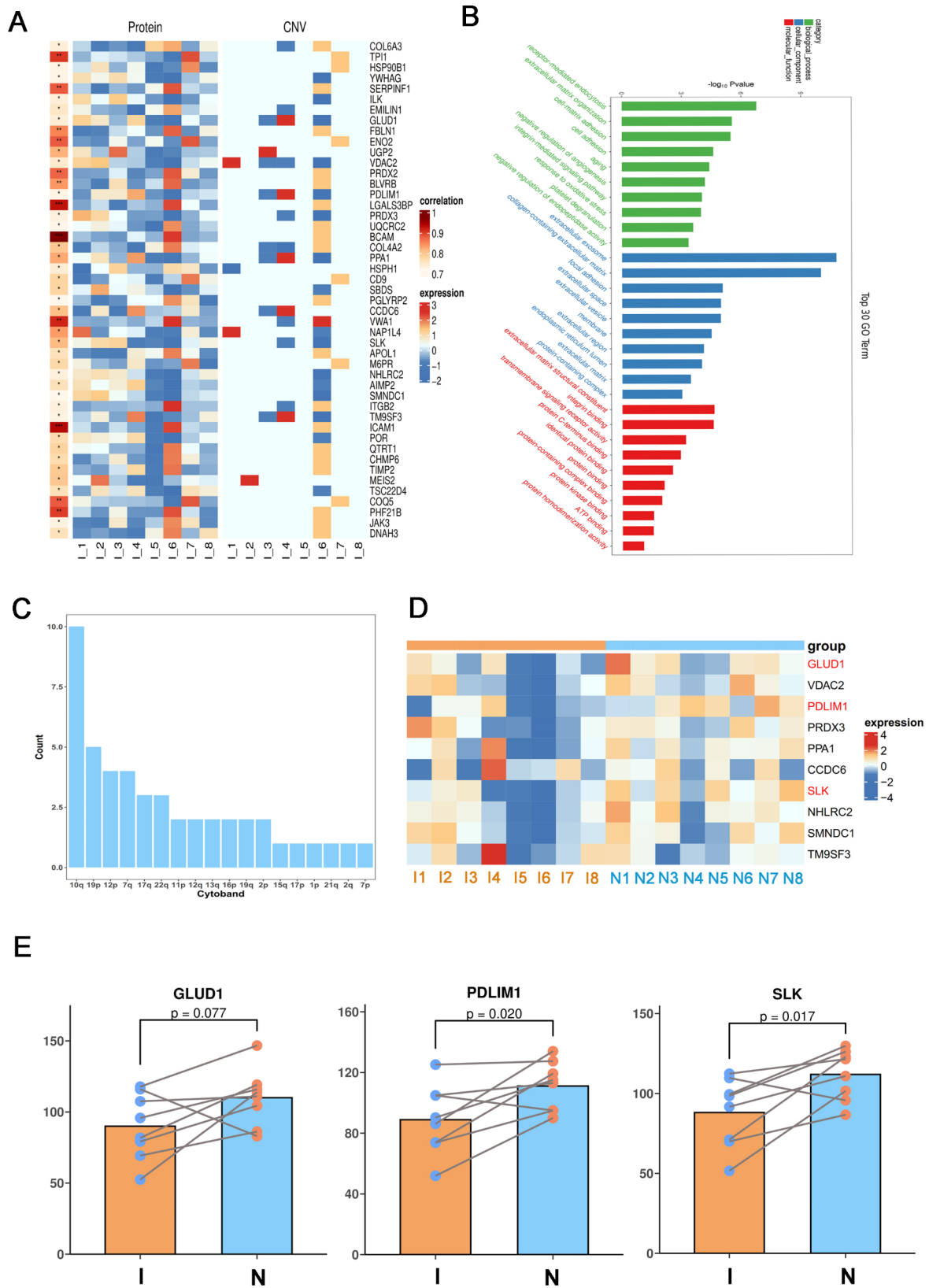


Fig. 6 Correlation analysis of TMT-based Quantitative Proteomics and whole-exosome sequencing. **(A)** Heatmap illustrating 47 positively related CNVs-DEPs. **(B)** Identification of the top 30 enriched GO terms related to CNVs-DEPs. **(C)** Distribution of cyto bands associated with CNVs-DEPs. **(D)** Presentation of 10 CNVs-DEPs with significant protein quantitation. **(E)** Quantification of the expression of three proteins (GLUD1, PDLIM1, and SLK) between IVL and normal myometrium

Table 1 Clinical characteristics and pathological changes in 23 IVL patients

Case	Tumor extension	Age (y)	hydropic change	Hyalinization	Vinculin expression	Morphology
1	Intrapelvic	47	minimal	minimal	middle	cellular
2	Intrapelvic	51	diffuse	focal	low	vascular
3	Intrapelvic	37	focal	minimal	low	usual
4	Intrapelvic	47	focal	focal	middle	cellular, vascular
5	Intrapelvic	47	minimal	minimal	high	vascular
6	Intrapelvic	52	focal	focal	low	cellular, vascular
7	Intrapelvic	59	minimal	diffuse	high	vascular
8	Intrapelvic	34	minimal	focal	high	vascular
9	Inferior Vena Cava	37	diffuse	diffuse	low	vascular
10	Inferior Vena Cava	44	focal	minimal	high	cellular
11	Inferior Vena Cava	48	diffuse	focal	high	vascular
12	Inferior Vena Cava	50	focal	focal	middle	vascular
13	Heart	30	diffuse	focal	low	vascular
14	Heart	42	diffuse	minimal	low	vascular
15	Heart	43	minimal	focal	low	vascular
16	Heart	45	focal	minimal	low	vascular, usual
17	Heart	47	minimal	focal	middle	vascular
18	Heart	50	focal	focal	low	vascular
19	Heart	55	minimal	diffuse	low	usual
20	Heart	59	minimal	minimal	low	vascular
21	Heart	62	focal	diffuse	middle	vascular
22	Lung	45	focal	diffuse	low	vascular
23	Lung	47	focal	focal	middle	vascular

Abbreviations

IVL	Intravenous leiomyomatosis
IVC	Inferior vena cava
UF	Uterine fibroid
SMCs	Smooth muscle cells
MED12	Mediator complex subunit 12
scRNA-seq	Single-cell RNA sequencing
H&E	Hematoxylin and eosin
IHC	Immunohistochemistry
TMT	Tandem mass tag
WES	Whole-Exome Sequencing
tSNE	t-distributed Stochastic Neighbor Embedding
GO	Gene Ontology
KEGG	Kyoto Encyclopedia of Genes and Genomes
DEPs	Differentially expressed proteins
CNV	Copy number variation
PPC	Percentage of positive cells
IS	Intensity of staining
ECM	Extracellular matrix

Supplementary Information

The online version contains supplementary material available at <https://doi.org/10.1186/s12967-024-05919-9>.

Supplementary Material 1

Acknowledgements

We thank all the patients enrolled in this study.

Author contributions

Jiarong Zhang, Yingyong Hou and Chunsheng Wang designed the study; Sheng Yin, Peipei Shi, Jing Han, Aimin Ren, Li Ma, Wenbin Tang, Hua Li, Wenxue Liu, Sihui Yu and Tingting Li collected the data; Sheng Yin, Peipei Shi and Jing Han analyzed the data; Sheng Yin and Peipei Shi wrote the original draft; Jiarong Zhang revised the manuscript. All authors approved the final paper.

Funding

This study was funded by the Zhongshan Development Program (XK-066).

Data availability

The primary data of genetics and proteomics has been deposited to the GSA-human database (<https://ngdc.cncb.ac.cn/gsa-human/>; ID: PRJCA015471) and OMIX (<https://ngdc.cncb.ac.cn/omix/>; OMIX003497), which is available from the corresponding author on request.

Declarations**Ethics approval and consent to participate**

The study was approved by the ethical committee of Zhongshan Hospital, Fudan University (Ethics Committee document number: B2021-488R). Written informed consent was obtained from all participating patients.

Consent for publication

Not applicable.

Competing interests

All authors declare no competing interests.

Received: 3 April 2024 / Accepted: 25 November 2024

Published online: 26 February 2025

References

1. CP HLK. Intravenous leiomyomatosis with cardiac extension: tumor thrombectomy through an abdominal approach. *J Vasc Surg.* 2000;31(5):1046–51.
2. Li H, Xu J, Lin Q, Zhang Y, Zhao Y, Tong H, et al. Surgical treatment strategies for extra-pelvic intravenous leiomyomatosis. *Orphanet J Rare Dis.* 2020;15(1):153.
3. Kir GKM, Gurbuz A, Karateke A, Aker F. Estrogen and progesterone expression of vessel walls with intravascular leiomyomatosis; discussion of histogenesis. *Eur J Gynaecol Oncol.* 2004;25(3):362–6.

4. Chen MJ, Peng Y, Yang YS, Huang SC, Chow SN, Torng PL. Increased hyaluronan and CD44 expressions in intravenous leiomyomatosis. *Acta Obstet Gynecol Scand*. 2005;84(4):322–8.
5. Lo KW, Lau TK. Intracardiac leiomyomatosis. Case report and literature review. *Arch Gynecol Obstet*. 2001;264(4):209–10.
6. Gashimova U. Histological examination of retinal function and the effects of curcuma longa on memory correction in experimental olfactory bulbectomy rat models. *Adv Biology Earth Sci*. 2024;9:216–22.
7. Miryusifova K. The saffron effects on the dynamics of experimental epilepsy. *Adv Biology Earth Sci*. 2024;9:196–202.
8. Ordulu Z, CH, Peng G, et al. Molecular and clinicopathologic characterization of intravenous leiomyomatosis. *Mod Pathol*. 2020;33(9):1844–60.
9. Lu B, Liu Q, Tang L, Ma Y, Shi H. Intravenous leiomyomatosis: molecular analysis of 17 cases. *Pathology*. 2020;52(2):213–7.
10. Wang L, Hu S, Xin F, Zhao H, Li G, Ran W, et al. MED12 exon 2 mutation is uncommon in intravenous leiomyomatosis: clinicopathologic features and molecular study. *Hum Pathol*. 2020;99:36–42.
11. Matsubara A, Sekine S, Yoshida M, Yoshida A, Taniguchi H, Kushima R, et al. Prevalence of MED12 mutations in uterine and extrauterine smooth muscle tumours. *Histopathology*. 2013;62(4):657–61.
12. Zhang X, Wu L, Xu R, Zhu C, Ma G, Zhang C, et al. Identification of the molecular relationship between intravenous leiomyomatosis and uterine myoma using RNA sequencing. *Sci Rep*. 2019;9(1):1442.
13. Goad J, Rudolph J, Zandigohar M, Tae M, Dai Y, Wei JJ, et al. Single-cell sequencing reveals novel cellular heterogeneity in uterine leiomyomas. *Hum Reprod*. 2022;37(10):2334–49.
14. Kalluri R, Zeisberg M. Fibroblasts in cancer. *Nat Rev Cancer*. 2006;6(5):392–401.
15. Tomasek JJ, Gabbiani G, Hinz B, Chaponnier C, Brown RA. Myofibroblasts and mechano-regulation of connective tissue remodelling. *Nat Rev Mol Cell Biol*. 2002;3(5):349–63.
16. De Martino D, Bravo-Cordero JJ. Collagens in Cancer: structural regulators and guardians of Cancer Progression. *Cancer Res*. 2023;83(9):1386–92.
17. Sahai E, Wyckoff J, Philippart U, Segall JE, Gertler F, Condeelis J. Simultaneous imaging of GFP, CFP and collagen in tumors in vivo using multiphoton microscopy. *BMC Biotechnol*. 2005;5:14.
18. Wishart AL, Conner SJ, Guarin JR, Fatherree JP, Peng Y, McGinn RA, et al. Decellularized extracellular matrix scaffolds identify full-length collagen VI as a driver of breast cancer cell invasion in obesity and metastasis. *Sci Adv*. 2020;6:43.
19. Graf F, Horn P, Ho AD, Boutros M, Maercker C. The extracellular matrix proteins type I collagen, type III collagen, fibronectin, and laminin 421 stimulate migration of cancer cells. *FASEB J*. 2021;35(7):e21692.
20. Robboy SJ, Bentley RC, Butnor K, Anderson MC. Pathology and pathophysiology of uterine smooth-muscle tumors. *Environ Health Perspect*. 2000;108(Suppl 5):779–84.
21. Wang W, Wang Y, Chen F, Zhang M, Jia R, Liu X, et al. Intravenous leiomyomatosis is inclined to a solid entity different from uterine leiomyoma based on RNA-seq analysis with RT-qPCR validation. *Cancer Med*. 2020;9(13):4581–92.
22. Pickup MW, Mouw JK, Weaver VM. The extracellular matrix modulates the hallmarks of cancer. *EMBO Rep*. 2014;15(12):1243–53.
23. Grashoff C, Hoffman BD, Brenner MD, Zhou R, Parsons M, Yang MT, et al. Measuring mechanical tension across vinculin reveals regulation of focal adhesion dynamics. *Nature*. 2010;466(7303):263–6.
24. Mouneimne G, Hansen SD, Selfors LM, Petrak L, Hickey MM, Gallegos LL, et al. Differential remodeling of actin cytoskeleton architecture by profilin isoforms leads to distinct effects on cell migration and invasion. *Cancer Cell*. 2012;22(5):615–30.
25. Zhang H, Yang W, Yan J, Zhou K, Wan B, Shi P, et al. Loss of profilin 2 contributes to enhanced epithelial-mesenchymal transition and metastasis of colorectal cancer. *Int J Oncol*. 2018;53(3):1118–28.
26. Schumacher S, Vazquez Nunez R, Biertümpfel C, Mizuno N. Bottom-up reconstitution of focal adhesion complexes. *Febs j*. 2022;289(12):3360–73.
27. Cristofolletti C, Picchio MC, Lazzeri C, Tocco V, Pagani E, Bresin A, et al. Comprehensive analysis of PTEN status in Sezary syndrome. *Blood*. 2013;122(20):3511–20.
28. van Thuijl HF, Scheinin I, Sie D, Alentorn A, van Essen HF, Cordes M, et al. Spatial and temporal evolution of distal 10q deletion, a prognostically unfavorable event in diffuse low-grade gliomas. *Genome Biol*. 2014;15(9):471.
29. Mao X, Yu Y, Boyd LK, Ren G, Lin D, Chaplin T, et al. Distinct genomic alterations in prostate cancers in Chinese and western populations suggest alternative pathways of prostate carcinogenesis. *Cancer Res*. 2010;70(13):5207–12.
30. Buza N, Xu F, Wu W, Carr RJ, Li P, Hui P. Recurrent chromosomal aberrations in intravenous leiomyomatosis of the uterus: high-resolution array comparative genomic hybridization study. *Hum Pathol*. 2014;45(9):1885–92.

Publisher's note

Springer Nature remains neutral with regard to jurisdictional claims in published maps and institutional affiliations.